Supplementary Information

Common dependency on stress for the two fundamental laws of statistical seismology

Clément Narteau[1], Svetlana Byrdina[1,2],
Peter Shebalin[1,3], Danijel Schorlemmer[4]

[1)] Institut de Physique du Globe de Paris (IPGP, UMR 7154, CNRS, Univ. P7), 4 Place Jussieu, Paris, Cedex 05, 75252, France.
[2)] Observatoire de Physique du Globe de Clermont-Ferrand (Univ. Blaise Pascal, IRD M163), 5 rue Kessler, 63038 Clermont-Ferrand, France.
[3)] International Institute of Earthquake Prediction Theory and Mathematical Geophysics, 84/32 Profsouznaya, Moscow 117997, Russia.
[4)] Department of Earth Sciences, University of Southern California, 3651 Trousdale Pkwy, Los Angeles, CA 90089, USA.

Contents

The underlying assumption of this work is that the aftershock rate results from the superposition of independent exponential decay rates with different characteristic time constants: these characteristic times to failure represent the time-dependent strength of the different seismogenic domains within the aftershock zone according to a mechanism of static fatigue [*Scholz*, 1968; *Narteau et al.*, 2002]. Hence, stacked aftershock sequences in various tectonic settings can be used to quantify such a time-dependent strength of the brittle crust. Here, we explore the effect of the stress environment on the early phase of the aftershock decay rate in southern California and Japan using data of the last decades.

1 Data processing

1.1 The declustering method

We use an earthquake catalogue of southern California containing relocated events with focal mechanisms from 1984 to 2003 [*Hauksson*, 2000] and the Southern California Seismic Network (SCSN) catalogue since 2003. We select only high-quality events with a solution misfit < 0.2 and a station distribution ratio ≥ 0.5. In Japan, we combine the F-Net catalogue with the JMA catalogue to isolate the focal mechanisms of main shocks since 1997 (F-Net) and their respective aftershocks (JMA).

To identify main shocks, we deselect earthquakes of magnitude smaller than M which are within a $0.020 \cdot 10^{0.50M}$ kilometre radius circle during the first $0.125 \cdot 10^{0.55M}$ days after a magnitude M event [*Gardner and Knopoff*, 1974; *Reasenberg*, 1985]. Using the same spatial scaling, earthquakes that precede larger events by less than 12 hours are classified as potential foreshocks and removed from the catalogue of main shocks. As a result, there are no overlapping aftershock sequences for the first 12 hours. For the remaining main shocks, corresponding aftershocks with no rake angle are extracted from the entire SCSN catalogue ($> 385\,000$ events between 1984–2007) and the JMA catalogue ($> 1\,100\,000$ events between 1997–2007). Practically, we select the smaller magnitude earthquakes occurring within 12 hours after a magnitude M main shock in a $0.02 \cdot 10^{0.50M}$ kilometre radius circle.

Finally, only 2% of the selected aftershocks are also present in the catalogues of seismicity with focal mechanisms. Thus, the dataset which is analysed here and in the manuscript is different from the catalogues of seismicity that have been used to determine the relationship between the b-value and the rake angle.

1.2 Determination of the magnitude thresholds for main shocks

We set the minimum magnitude threshold for main shocks $M_{\min}^{\mathrm{M}} = 2.5$ as this is the overall completeness level of the relocated catalogue of focal

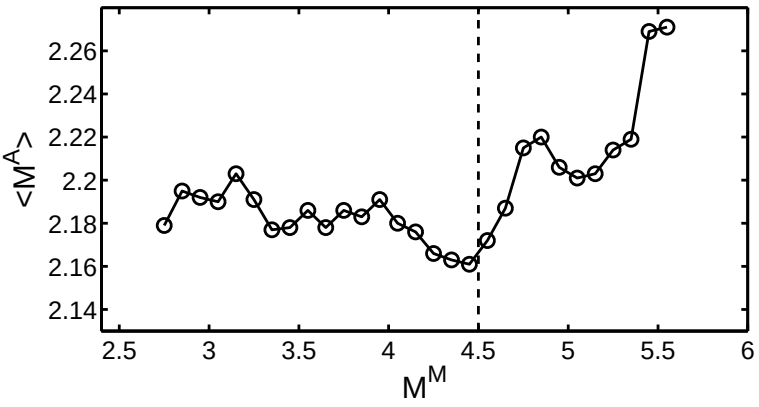

Figure 1: The average magnitude of aftershocks ranging from 1.8 to 2.5 with respect to the magnitude of their main shocks. Magnitude ranges of main shocks are determined by a sliding window with a width of 0.5 that moves from 2.5 to 5.3 by step of 0.1. The M^{M}-value is the centre of this sliding window. The average magnitude of aftershocks increases systematically for $M^{\mathrm{M}} > 4.5$ (overlapping records) but remains stable for lower M^{M}-values. This stable behaviour suggests that, using main shocks ranging in magnitudes from $M^{\mathrm{M}}_{\mathrm{min}}$ to 4.5, the estimation of the c-value can be performed on aftershock catalogues for which the completeness does not seem to change.

mechanism [*Schorlemmer et al.*, 2005].

To determine $M^{\mathrm{M}}_{\mathrm{max}}$, the maximum main-shock magnitude threshold, we examine the magnitude from which overlapping records start to systematically influence the earthquake-size distribution of the smaller aftershocks in the southern Californian catalogue. Then, we analyse a single magnitude range of aftershocks from 1.8 to 2.5. Classes of main shocks are formed using a sliding window of width 0.5 that moves in 0.1 unit steps from $M^{\mathrm{M}}_{\mathrm{min}}$ to 5.3. For each class, we generate the corresponding list of aftershocks in $[1.8, 2.5]$, and estimate $\langle M^{\mathrm{A}} \rangle$, the average magnitude of these aftershocks. Fig. 1 shows variations of the $\langle M^{\mathrm{A}} \rangle$-value according to the magnitude of the main shocks. For an increasing main-shock magnitude, the $\langle M^{\mathrm{A}} \rangle$-value is generally increasing if $M^{\mathrm{M}} > 4.5$ because smaller aftershocks are increasingly missing in the stacks. Below this threshold, the $\langle M^{\mathrm{A}} \rangle$-value oscillates around an equilibrium value indicating that the impact of overlapping records on catalogue completeness is stationary; therefore, we set $M^{\mathrm{M}}_{\mathrm{max}} = 4.5$.

1.3 The c-value with respect to the average magnitude of aftershocks

Aftershocks selected through our declustering method are used to determine c-values. First, we stack aftershocks according to the time passed from their respective main shocks. Then, we evaluate the c-value separately for different magnitude ranges of aftershocks by a maximum-likelihood method using continuous minimisation by simulated annealing [*Narteau et al.*, 2002].

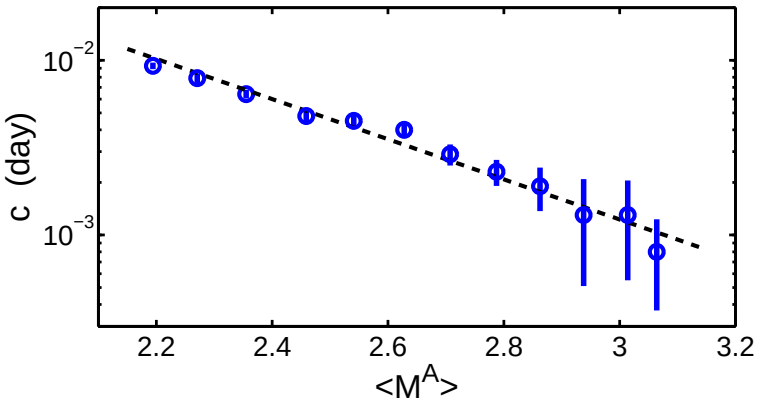

Figure 2: Evolution of the c-value with respect to the average magnitude of aftershocks triggered by $3 < M^{\mathrm{M}} < 3.5$ main shocks. The c-value and the $\langle M^{\mathrm{A}} \rangle$-value are calculated from stacked aftershock sequences in various magnitude ranges. These magnitude ranges of aftershocks are determined by a sliding window with a width of 1 magnitude unit that moves from 1.8 to 3.1 by step of 0.1. The linear regression line is $c = 0.54 - 1.15\langle M^{\mathrm{A}} \rangle$. Error bars are estimated by a Monte Carlo method and correspond to 16% and 84% quantiles of the maximum-likelihood estimates of c for 500 synthetic aftershock sequences at each point.

Fig. 2 shows that the characteristic time before the power-law decay starts is continuously decreasing as the average magnitude of aftershocks is increasing. A similar relationship has been reported for individual earthquakes in California and Japan [*Shcherbakov et al.*, 2004; *Nanjo et al.*, 2007].

These observations explain the difference in the c-value with respect to the average aftershock magnitude. In principle, for large-magnitude main shocks and small-magnitude aftershocks, such a variation of the c-value can be also an artefact due to a deficit of smaller events in the catalogues over short times. This is the reason why we only study the large aftershocks of intermediate-magnitude main shock in zones where the detection threshold is lower than the minimum threshold magnitude for aftershock selection. Thus, artefacts arising from overlapping records are considerably reduced (see Sec. 3). Furthermore, the dependence of the c-value to the rake angle is present in every magnitude range of aftershocks (Figs. 9 and 10). In this case, absolute variations of the mean c-value can be entirely separated from the behaviour exposed in the manuscript.

2 Spatial and temporal distributions of aftershocks

Fig. 3 shows the spatial distribution of main shocks and the temporal distribution of aftershocks in southern California for normal, strike-slip, and thrust main shocks. For the temporal distribution of aftershocks (Figs. 3a and 3b), we divide our aftershock catalogue into three subcatalogues ac-

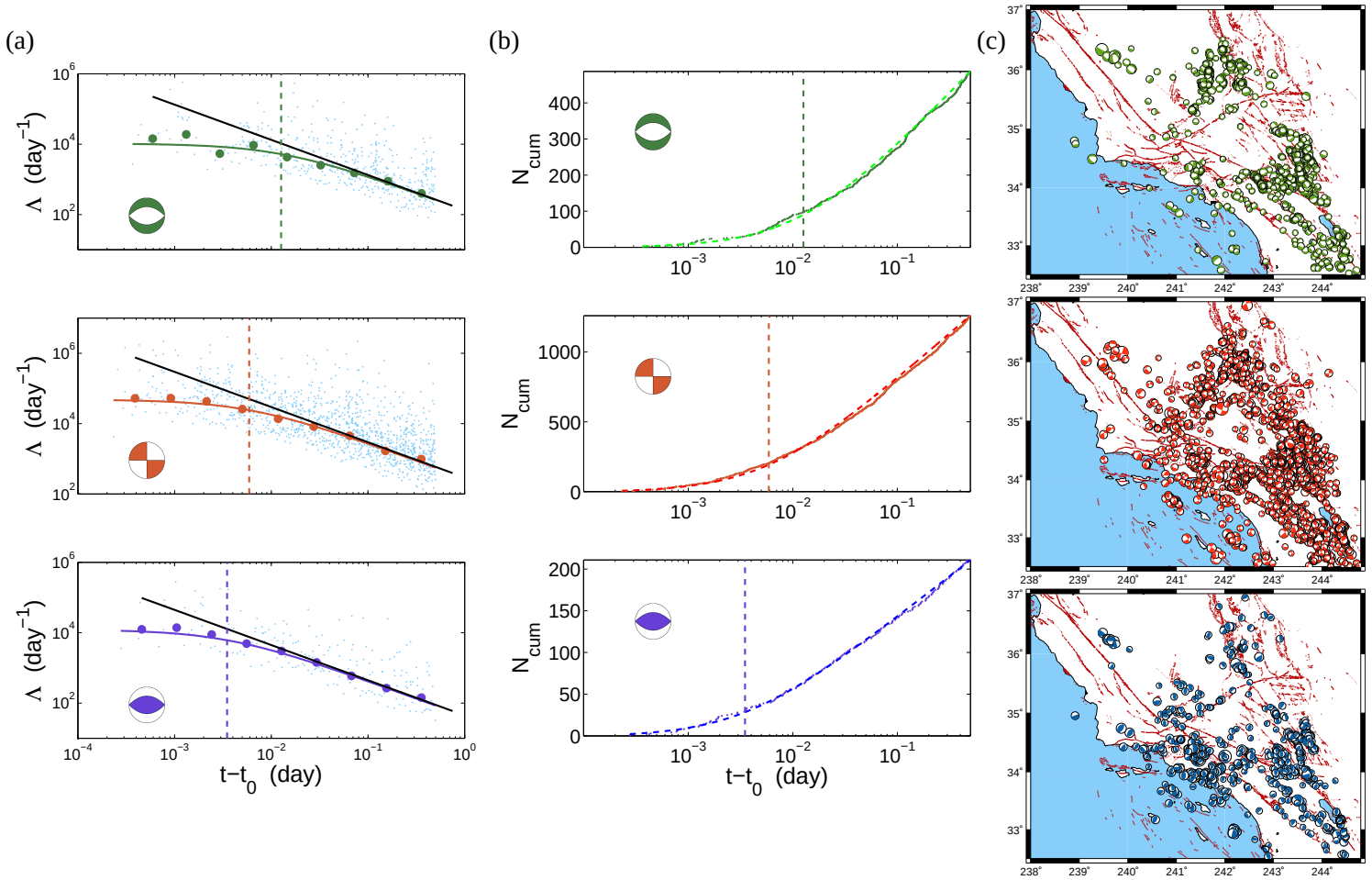

Figure 3: Spatial distribution of main shocks and temporal distribution of aftershocks for normal (top), strike-slip (bottom), and thrust (bottom) events: **(a)** The aftershock frequency with respect to the time from the main shock in double logarithmic scale. The coordinates of the small dots are $(\sqrt{t_{i+1}t_i}, 1/(t_{i+1}-t_i))$ where t_i is the time of the i^{th} aftershocks. Large dots correspond to the mean frequency averaged in time bins of equal duration in logarithmic scale. The colored solid lines correspond to the best fits of the data. The black line corresponds to a $1/t$ hyperbolic decay rate. The vertical dashed line indicates the c-value. **(b)** The cumulative number of events with respect to the logarithm of the time from the main shock. The dashed line corresponds to the best fits of the data. For individual sequence, the distance between the solid and dashed line is a good indication of the quality of fit. The vertical dashed line indicates the c-value. **(c)** Spatial disribution and focal mechanism of $2.5 < M^{\mathrm{M}} < 4.5$ main shocks.

	$M^{\rm M}_{\rm min} = 3.0;\ M^{\rm M}_{\rm max} = 4.5$					
	$M^{\rm A}_{\rm min} = 0.8$	$M^{\rm A}_{\rm min} = 1.2$	$M^{\rm A}_{\rm min} = 1.8$			$M^{\rm A}_{\rm min} = 2.4$
	$t > 0$	$t > 0$	$t > 0$	$t < 5 \cdot 10^{-4}$	$t > 5 \cdot 10^{-4}$	$t > 0$
Peng et al. (2007)	269	113	32	6	26	12
JMA	183	87	26	1	25	12
$P_{\rm rec}$	0.68	0.77	0.81	0.17	0.96	1.00

Table 1: Comparison of the number of aftershocks between the hand-picked catalogue of *Peng et al.* [2007] and the JMA catalogue. The corresponding 77 main shocks have magnitudes ranging from $M^{\rm M}_{\rm min} = 3.0$ to $M^{\rm M}_{\rm min} = 4.5$. $P_{\rm rec}$ is the probability for an event to be recorded in the JMA catalogue derived from the number of recorded events in both catalogues. The magnitude of the largest missing aftershock is equal to 2.3 (i. e. all $M^{\rm A} \geq 2.4$ aftershocks are recorded in the JMA catalogue). There is an increasing number of missing aftershocks for a decreasing $M^{\rm A}_{\rm min}$-value. For $M^{\rm A}_{\rm min} = 1.8$ the catalogue is almost complete after $5 \cdot 10^{-4}$ day (see also Fig. 4).

cording to λ, the rake angle of the main shocks. Normal events have $-135° \leq \lambda \leq -45°$; strike-slip have $-45° \leq \lambda \leq 45°$, $-180° \leq \lambda \leq -135°$, and $135° \leq \lambda \leq 180°$; thrust have $45° \leq \lambda \leq 135°$. Fig. 3a shows the variability of the aftershock rate over time and how a clear decay rate emerges when the frequency of events is averaged over time bins of equal duration in logarithmic scale. In this case, we can visually estimate the c-value and verify that the time delay before the onset of the power-law aftershock decay rate is increasing going from normal over strike-slip to thrust events. Finally, Fig. 3b shows the cumulative number of events with respect to the logarithm of the time from the main shock. The difference between the data and the best fit gives a good indication of the quality of our estimation procedure.

For the spatial distribution of main shocks, Fig. 3c shows that all types of focal mechanisms are well distributed across southern California. This is essentially due to the fact that we are working on small magnitude events and that there is everywhere some local complexity in fault structure despite the predominance of strike-slip faults.

3 Aftershock catalogue completeness

Missing aftershocks can strongly affect the evaluation of the time delay before the onset of the power-law aftershock decay rate. In Japan, we take

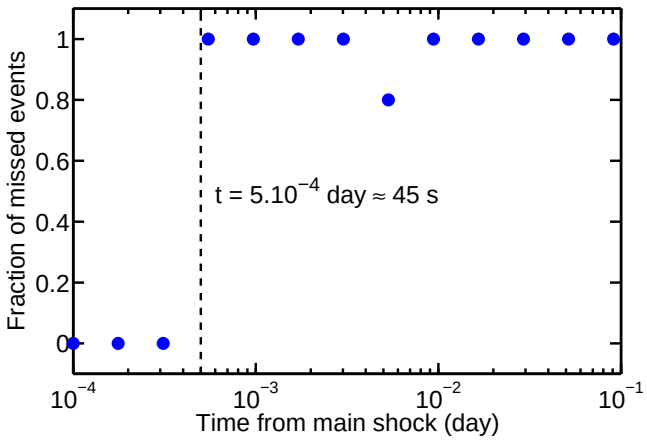

Figure 4: Ratio between $M^{\mathrm{A}} > 1.8$ aftershocks listed in the JMA catalogue and events picked by *Peng et al.* [2007] in time bins of equal duration in logarithmic scale (see also Fig. 7 of *Peng et al.* [2007]). The catalogue can be considered complete after $5 \cdot 10^{-4}$ day.

advantage of the hand-picked catalogue obtained by *Peng et al.* [2007] to quantify the proportion of recorded events and estimate the role of missing aftershocks in the estimation of the c-value.

Tab. 1 compares the number of recorded events in the JMA and the Peng catalogues. For $3.0 < M^{\mathrm{M}} < 4.5$ main shocks and $M^{\mathrm{A}} > 2.3$ aftershocks, the JMA can be assumed to be complete as the number of events is the same. Then, Fig. 5 shows that, for these magnitude ranges, we are able to identify a dependency of the c-value on the rake angle: the c-value is larger for normal events, smaller for thrust ones, and takes intermediate values for strike-slip events. Compared to southern California, the smaller c-values and the more instable behaviour observed in Japan may be explained by a larger average main-shock magnitude and a smaller number of main shocks.

For $M^{\mathrm{A}} > 1.8$ aftershocks, Tab. 1 and Fig. 4 show that more than 80% of the aftershocks are listed in the JMA catalogue as the probability for an event to be recorded switches rapidly from 0 to 1 after $5 \cdot 10^{-4}$ day (i. e. 45 secondes). Interestingly, this change in completeness over time can be used to provide a better estimate of the c-value and to quantify the effect of missing events on the evaluation of c.

Let us point out some basic properties of the optimisation procedure that depend on two values:

- T_{comp} the time at which the catalogue is complete,
- T_{start} the time at which we start the fit.

It is evident that, if $c < T_{\mathrm{comp}}$, the estimated c-value cannot be considered as reliable. In case $c < T_{\mathrm{start}}$, the error on the c-value is large and increases exponentially with T_{start}. In case $T_{\mathrm{start}} < T_{\mathrm{comp}} < c$, the c-value

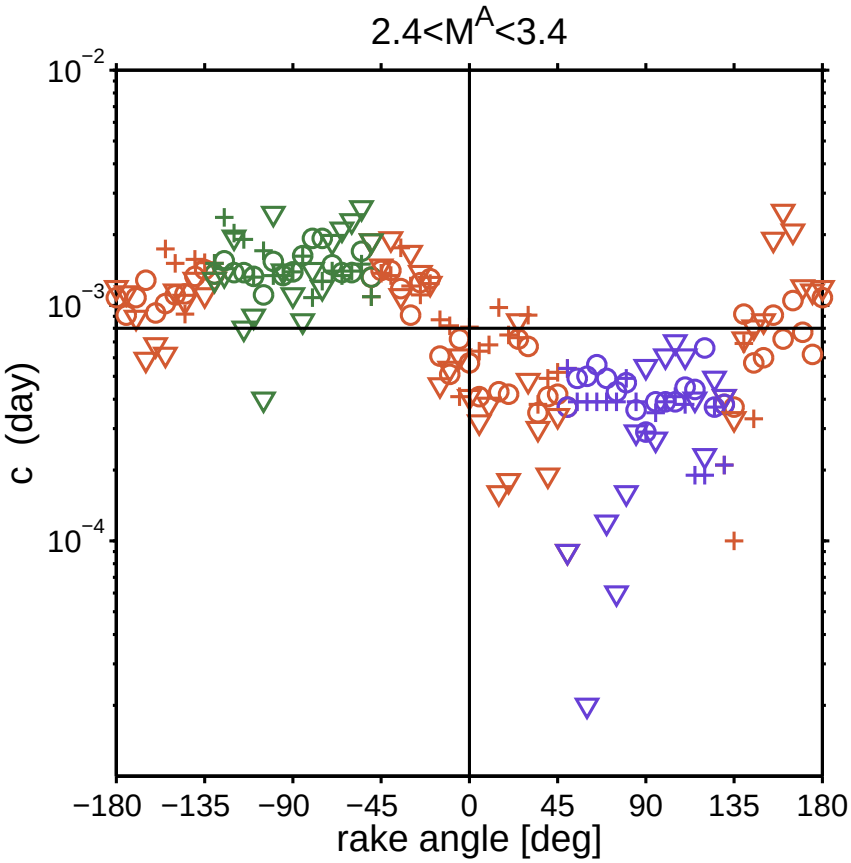

Figure 5: The logarithm of the c-value with respect to the first ($+$), the second ($\triangledown$) and both rake angles ($\circ$) for $2.4 < M^{\mathrm{A}} < 3.4$ aftershocks in Japan. Main shocks are classified according to their rake angles λ using a sliding window with a width of 60° and a step size of 5°. Green is for $-135^\circ \leq \lambda \leq -45^\circ$ (normal events); red is for $-45^\circ \leq \lambda \leq 45^\circ$, $-180^\circ \leq \lambda \leq -135^\circ$, and $135^\circ \leq \lambda \leq 180^\circ$ (strike-slip events); blue is for $45^\circ \leq \lambda \leq 135^\circ$ (thrust events).

may be overestimated because of catalogue incompleteness. Therefore, the preferable conditions for the estimation of the c-value is $T_{\rm comp} < T_{\rm start} < c$.

Using the hand-picked catalogue of *Peng et al.* [2007], we can determine the c- and $T_{\rm comp}$-values to verify that for different magnitude ranges of these aftershock sequences $c > T_{\rm comp}$. Then, using the events listed in the JMA catalogue, Fig. 7 shows how it is possible to use an increasing $T_{\rm start}$-value to converge toward a good estimation of the c-values (i. e. the c-values obtained from the hand-picked catalogue). This convergence depends on the proportion of recorded events (see Tab. 1 and Figs. 7a, 7b, and 7c) but also on their distribution over time (see Fig. 4 and Fig. 7 of *Peng et al.* [2007]). For $1.8 < M^{\rm A} < 2.8$ aftershocks, it is recommended to take $T_{\rm start} = 5 \cdot 10^{-4}$ day because this is the time at which the proportion of recorded events switches rapidly from 0 to 1. Then, for these events also, the c-value is larger for normal events, smaller for thrust ones, and takes intermediate values for strike-slip events (Fig. 6).

Most importantly, for any aftershock catalogue for which the level of completeness is not well defined, it is possible to use the starting time of the optimisation procedure to estimate the stability of the c-value and verify that missing aftershocks do not perturb the estimation of this parameter. For southern California. Fig. 8 shows that for $T_{\rm start} = 10^{-4}$ day (9 seconds), $T_{\rm start} = 5 \cdot 10^{-4}$ day (45 seconds), $T_{\rm start} = 10 \cdot 10^{-4}$ day (90 seconds), and $T_{\rm start} = 14 \cdot 10^{-4}$ day (2 minutes) there is no significant change in the estimation of c-values for all classes of rake angles. As the catalogue of $M^{\rm A} > 1.8$ aftershocks is complete 2 minutes after a $M^{\rm M} < 4.5$ main shock [*Kilb et al.*, 2007], this stability in the c-value clearly indicates that the missing aftershocks do not affect the estimation of this parameter in this particular case (i. e. $T_{\rm comp} < T_{\rm start} < c$ for all considered parameters including different rake angles).

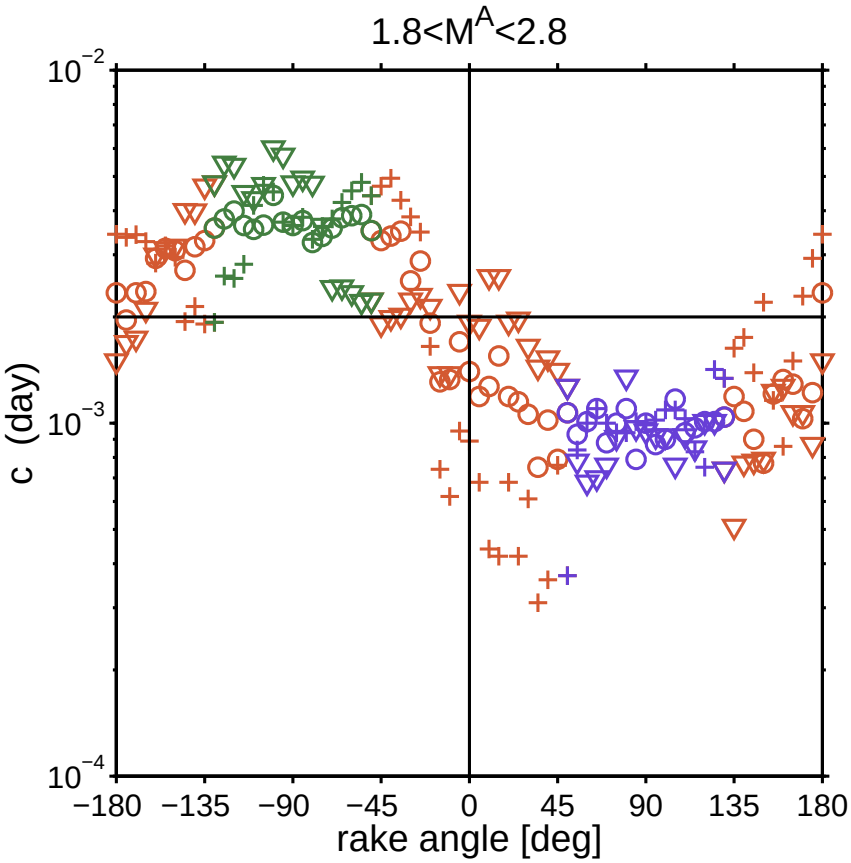

Figure 6: The logarithm of the c-value with respect to the first ($+$), the second ($\triangledown$) and both rake angles ($\circ$) for $1.8 < M^{\mathrm{A}} < 2.8$ aftershocks in Japan taking $T_{\mathrm{start}} = 5 \cdot 10^{-4}$ day. Main shocks are classified according to their rake angles λ using a sliding window with a width of 60° and a step size of 5°. Green is for $-135^\circ \leq \lambda \leq -45^\circ$ (normal events); red is for $-45^\circ \leq \lambda \leq 45^\circ$, $-180^\circ \leq \lambda \leq -135^\circ$, and $135^\circ \leq \lambda \leq 180^\circ$ (strike-slip events); blue is for $45^\circ \leq \lambda \leq 135^\circ$ (thrust events).

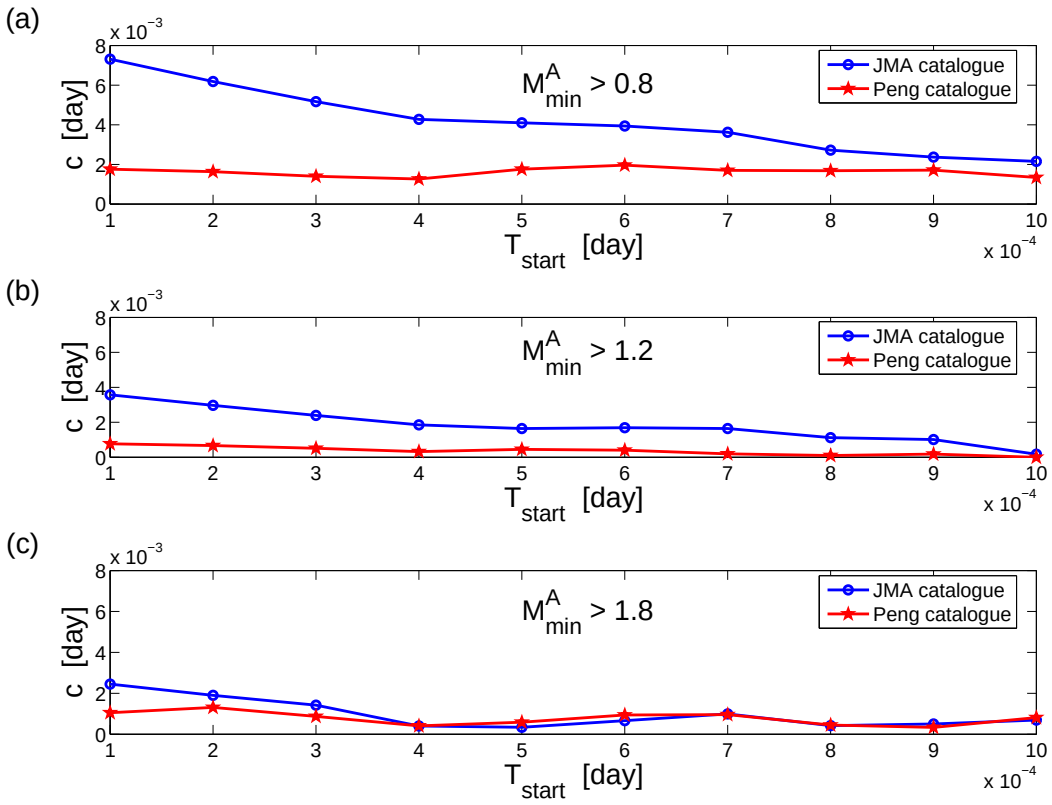

Figure 7: Comparison between c-values obtained from the catalogue of *Peng et al.* [2007] and the JMA catalogue with respect to $T_{\rm start}$, the starting time of the optimisation procedure: (a) $M^{\rm A}_{\rm min} = 0.8$, (b) $M^{\rm A}_{\rm min} = 1.2$, (c) $M^{\rm A}_{\rm min} = 1.8$. The c-value for the hand-picked catalogue is smaller and stable. Thus, we verify that $c > T_{\rm start}$. The c-value for the JMA catalogue decreases and systematically tends to the c-value of the hand-picked catalogue due to a decreasing proportion of missing aftershocks in the stacks. For an increasing $M^{\rm A}_{\rm min}$-value, the difference between both c-values decreases. For $M^{\rm A}_{\rm min} = 1.8$, this difference is extremely small and negligible for $T_{\rm start} \geq 4 \cdot 10^{-4}$ day.

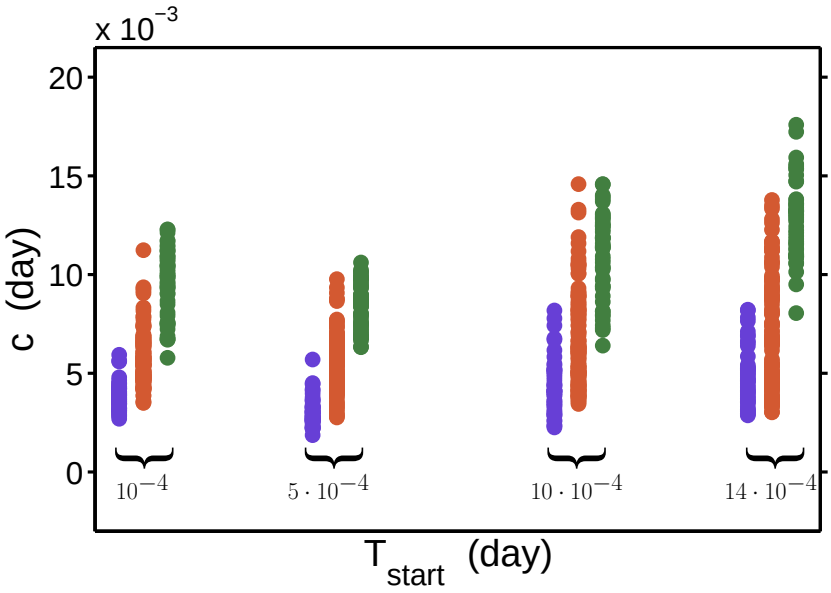

Figure 8: The c-values with respect to $T_{\text{start}} \in [10^{-4}; 5{\cdot}10^{-4}; 10{\cdot}10^{-4}; 14{\cdot}10^{-4}]$ according to the rake angles, λ, of the main shocks. Green is for $-135^\circ \leq \lambda \leq -45^\circ$ (normal events); red is for $-45^\circ \leq \lambda \leq 45^\circ$, $-180^\circ \leq \lambda \leq -135^\circ$, and $135^\circ \leq \lambda \leq 180^\circ$ (strike-slip events); blue is for $45^\circ \leq \lambda \leq 135^\circ$ (thrust events). The higher variability for higher T_{start}-values results from the smaller number of aftershocks in the stacks. There is no systematic trend associated with the T_{start}-value as we observe that the major contribution on the variation of the c-value is the rake angle λ. These results indicate that, in southern California, the dependency of the c-value on the rake angle is not an artefact of catalogue incompleteness.

4 Rake angles and aftershock magnitude ranges

Figs. 9 and 10 show the evolution of the logarithm of the c-value with respect to the first, the second, and both rake angles for 4 different magnitude ranges of aftershocks in southern California. In Fig. 10, main shocks are classified according to their rake angles using a sliding window with a width of 40° instead of 60°. The use of both rakes simultaneously multiplies artificially the number of data by a factor 2, symmetrises the results but keeps unchanged the faulting style. Note that fluctuations in c-values are higher with an increasing aftershock magnitude. Such a behaviour results only from the smaller number of events in the stacks (see error bars in Figs. 11 and 12). In addition, the level of noise is always higher when using rake 2 instead of rake 1. This is particularly the case for strike-slip events with a rake angle around 180°. It indicates that the choice of the first and second rake is not purely random, the first being the most reliable one.

Fig. 11 shows the evolution of the c-value with respect to the first rake angle for two aftershock ranges ([1.8, 2.8] and [2.4, 3.4]) in southern California. For these two ranges, Figs. 11b and 11c show the number of selected aftershock and the average magnitudes of selected main shocks and aftershocks. In a similar manner, Fig. 12 shows the evolution of the same parameters with respect to the second rake angle. Figs. 11 and 12 have to be compared with the Fig. 1 of the manuscript.

For the same magnitude ranges as in California, Figs. 13, 14 and 15 show the evolution of the c-value in Japan with respect to the first, the second and both rake angles, respectively. Figs. 13b, 14b, 15b, 13c, 14c, and 15c show also the number of selected aftershocks and the average magnitudes of selected main shocks and aftershocks.

Not surprisingly, southern California seismicity is dominated by strike-slip events and Japanese seismicity is dominated by thrust and normal events. For Japan, the F-Net catalogue starts in 1997 and contains only few events of $M^{\mathrm{M}} < 3.5$ (see the Tab. 1 in *Schorlemmer et al.* [2005]). As a consequence, the average main shock magnitude is higher in Japan than in southern California for $2.5 < M^{\mathrm{M}} < 4.5$ main shocks. Subsequently, aftershock magnitudes are also higher and the resulting c-values are smaller. It is therefore impossible to directly compare the c-values obtained for the same magnitude ranges in Japan and in southern California. Nevertheless, the common dependency of the b- and c-values on the rake angle is observed in both regions.

In Japan and southern California, we still have to explore the dependency of the c- and b-values with respect to depth for each of the different faulting regimes.

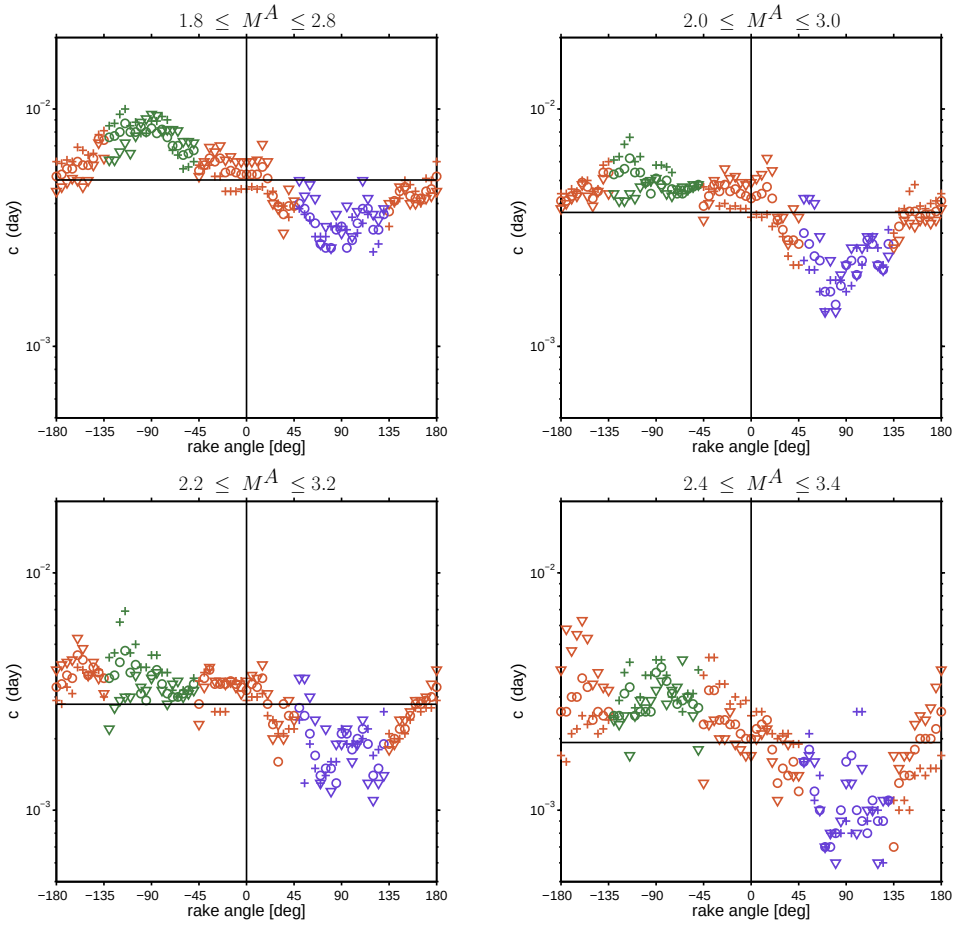

Figure 9: The logarithm of the c-value with respect to the first (+), the second ($\triangledown$) and both rake angles ($\circ$) for different magnitude ranges of aftershocks in southern California. As in the manuscript, main shocks are classified according to their rake angles λ using a sliding window with a width of 60° and a step size of 5°. Green is for $-135^\circ \leq \lambda \leq -45^\circ$ (normal events); red is for $-45^\circ \leq \lambda \leq 45^\circ$, $-180^\circ \leq \lambda \leq -135^\circ$, and $135^\circ \leq \lambda \leq 180^\circ$ (strike-slip events); blue is for $45^\circ \leq \lambda \leq 135^\circ$ (thrust events).

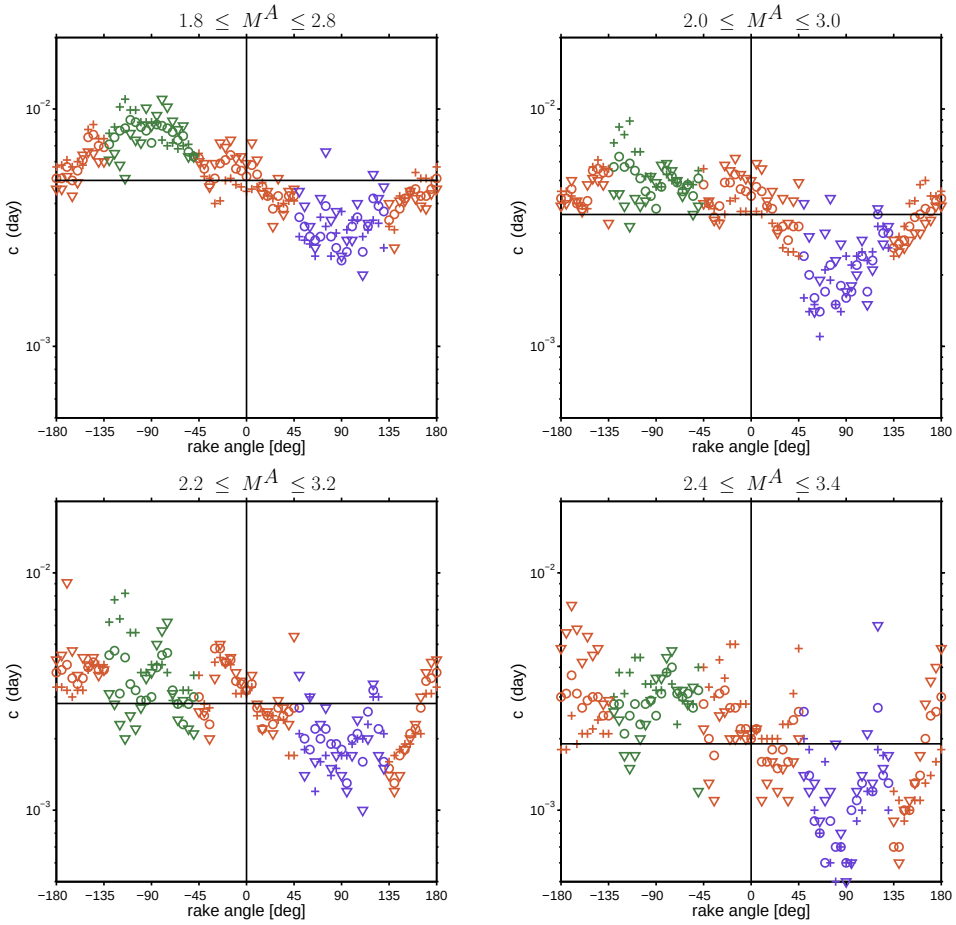

Figure 10: The logarithm of the c-value with respect to the first (+), the second ($\triangledown$) and both rake angles ($\circ$) for different magnitude ranges of aftershocks in southern California. Main shocks are classified according to their rake angles λ using a sliding window with a width of 40° and a step size of 5°. Green is for $-135^\circ \leq \lambda \leq -45^\circ$ (normal events); red is for $-45^\circ \leq \lambda \leq 45^\circ$, $-180^\circ \leq \lambda \leq -135^\circ$, and $135^\circ \leq \lambda \leq 180^\circ$ (strike-slip events); blue is for $45^\circ \leq \lambda \leq 135^\circ$ (thrust events).

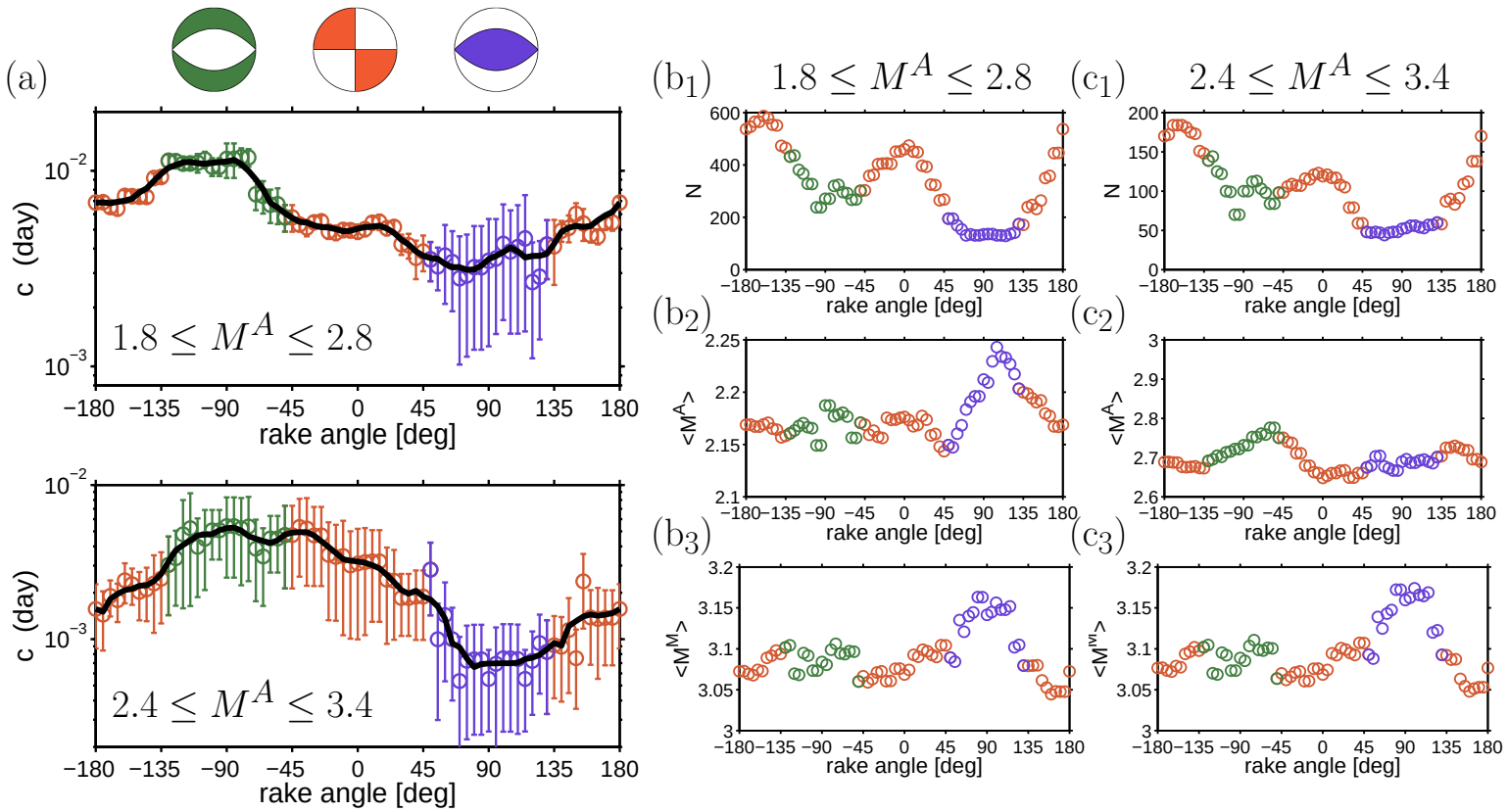

Figure 11: **(a)** the logarithm of the c-value with respect to the first rake angle for aftershock-magnitude ranges of $[1.8; 2.8]$ (top) and $[2.4; 3.4]$ (bottom) in southern California. Red, green and blue distinguish rake intervals of mainly strike-slip, normal, and thrust events, respectively. Error bars are estimated by a Monte Carlo method and correspond to 16% and 84% quantiles of the maximum-likelihood estimates of c for 500 synthetic aftershock sequences at each point. **(b)** and **(c)** show the number of selected aftershocks (b_1 and c_1), the average magnitude of selected aftershocks (b_2 and c_2), and selected main shocks (b_3 and c_3).

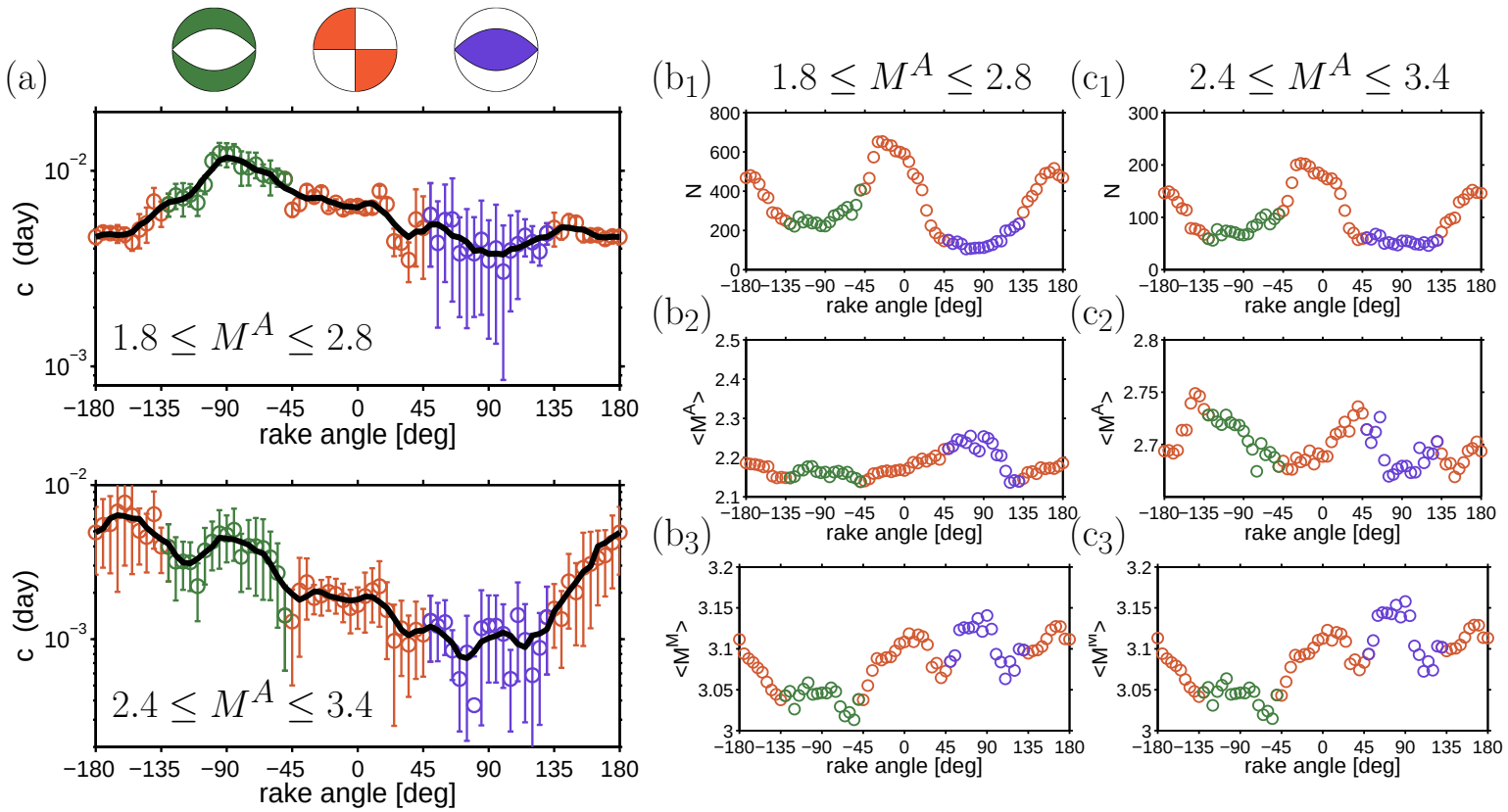

Figure 12: **(a)** the logarithm of the c-value with respect to the second rake angle for aftershock-magnitude ranges of $[1.8; 2.8]$ (top) and $[2.4; 3.4]$ (bottom) in southern California. Red, green and blue distinguish rake intervals of mainly strike-slip, normal, and thrust events, respectively. Error bars are estimated by a Monte Carlo method and correspond to 16% and 84% quantiles of the maximum-likelihood estimates of c for 500 synthetic aftershock sequences at each point. **(b)** and **(c)** show the number of selected aftershocks (b_1 and c_1), the average magnitude of selected aftershocks (b_2 and c_2), and selected main shocks (b_3 and c_3).

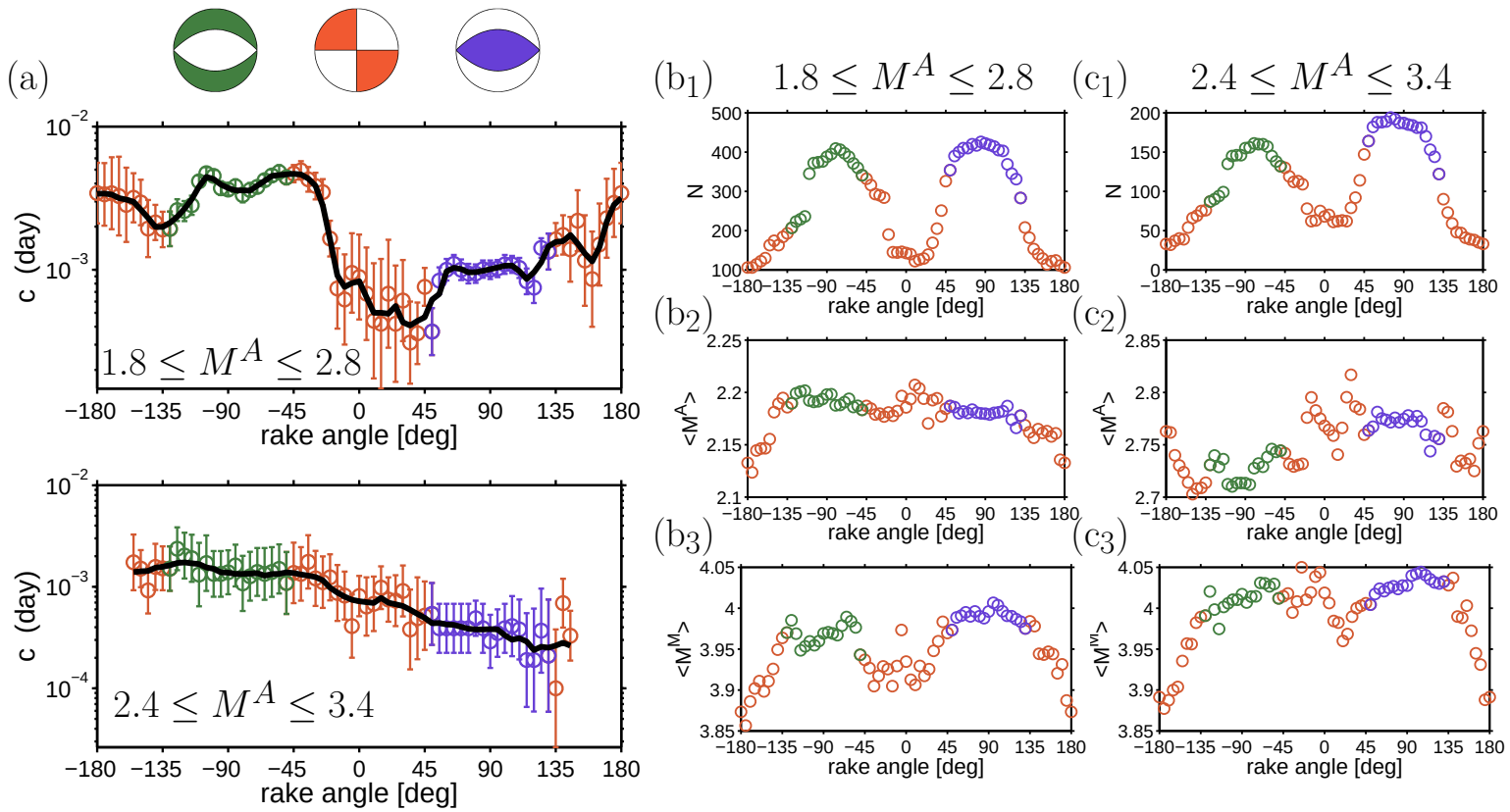

Figure 13: **(a)** the logarithm of the c-value with respect to the first rake angle for aftershock-magnitude ranges of $[1.8; 2.8]$ (top) and $[2.4; 3.4]$ (bottom) in Japan. Red, green and blue distinguish rake intervals of mainly strike-slip, normal, and thrust events, respectively. Error bars are estimated by a Monte Carlo method and correspond to 16% and 84% quantiles of the maximum-likelihood estimates of c for 500 synthetic aftershock sequences at each point. **(b)** and **(c)** show the number of selected aftershocks (b_1 and c_1), the average magnitude of selected aftershocks (b_2 and c_2), and selected main shocks (b_3 and c_3).

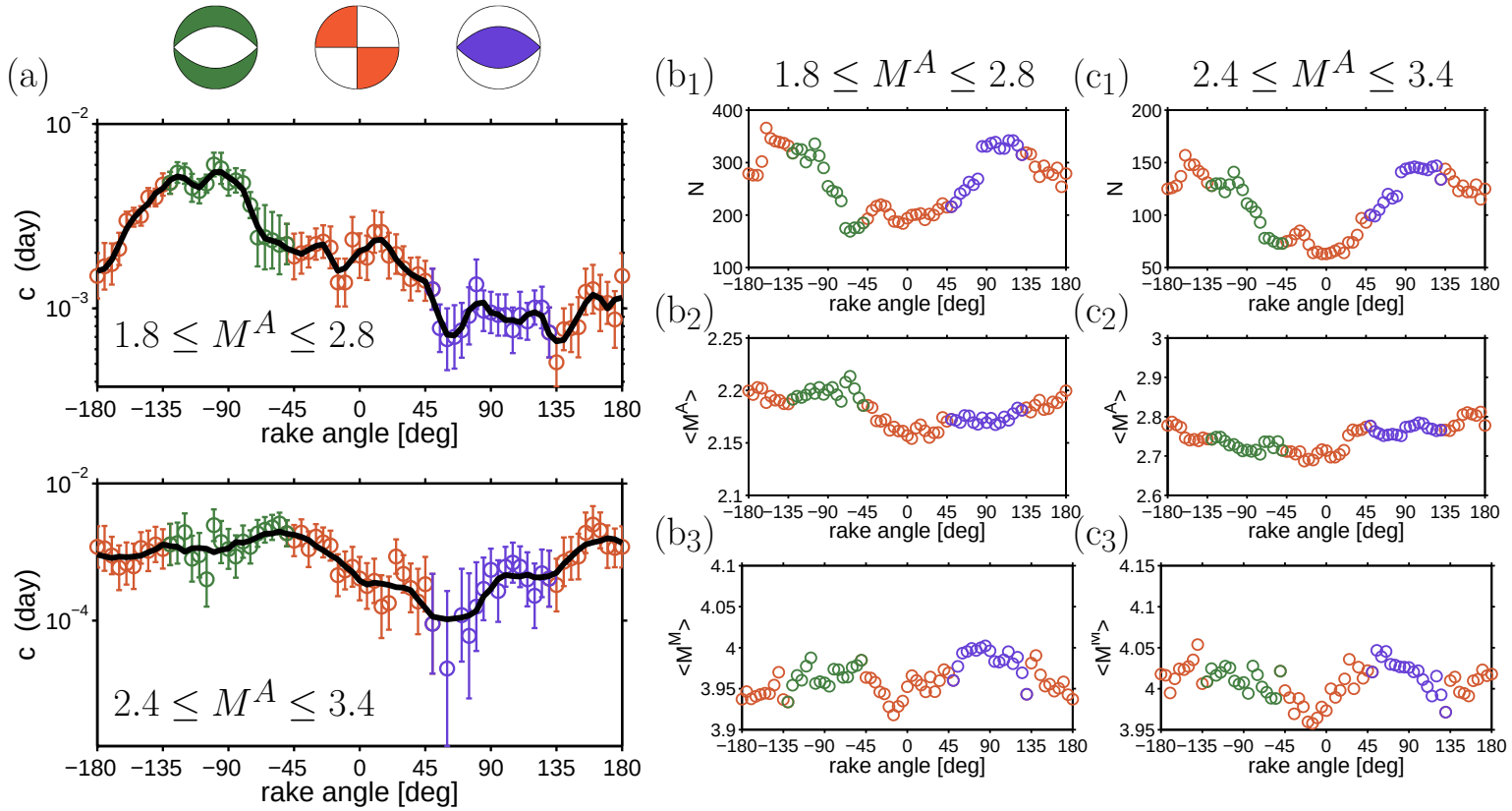

Figure 14: **(a)** the logarithm of the c-value with respect to the second rake angle for aftershock-magnitude ranges of $[1.8; 2.8]$ (top) and $[2.4; 3.4]$ (bottom) in Japan. Red, green and blue distinguish rake intervals of mainly strike-slip, normal, and thrust events, respectively. Error bars are estimated by a Monte Carlo method and correspond to 16% and 84% quantiles of the maximum-likelihood estimates of c for 500 synthetic aftershock sequences at each point. **(b)** and **(c)** show the number of selected aftershocks (b_1 and c_1), the average magnitude of selected aftershocks (b_2 and c_2), and selected main shocks (b_3 and c_3).

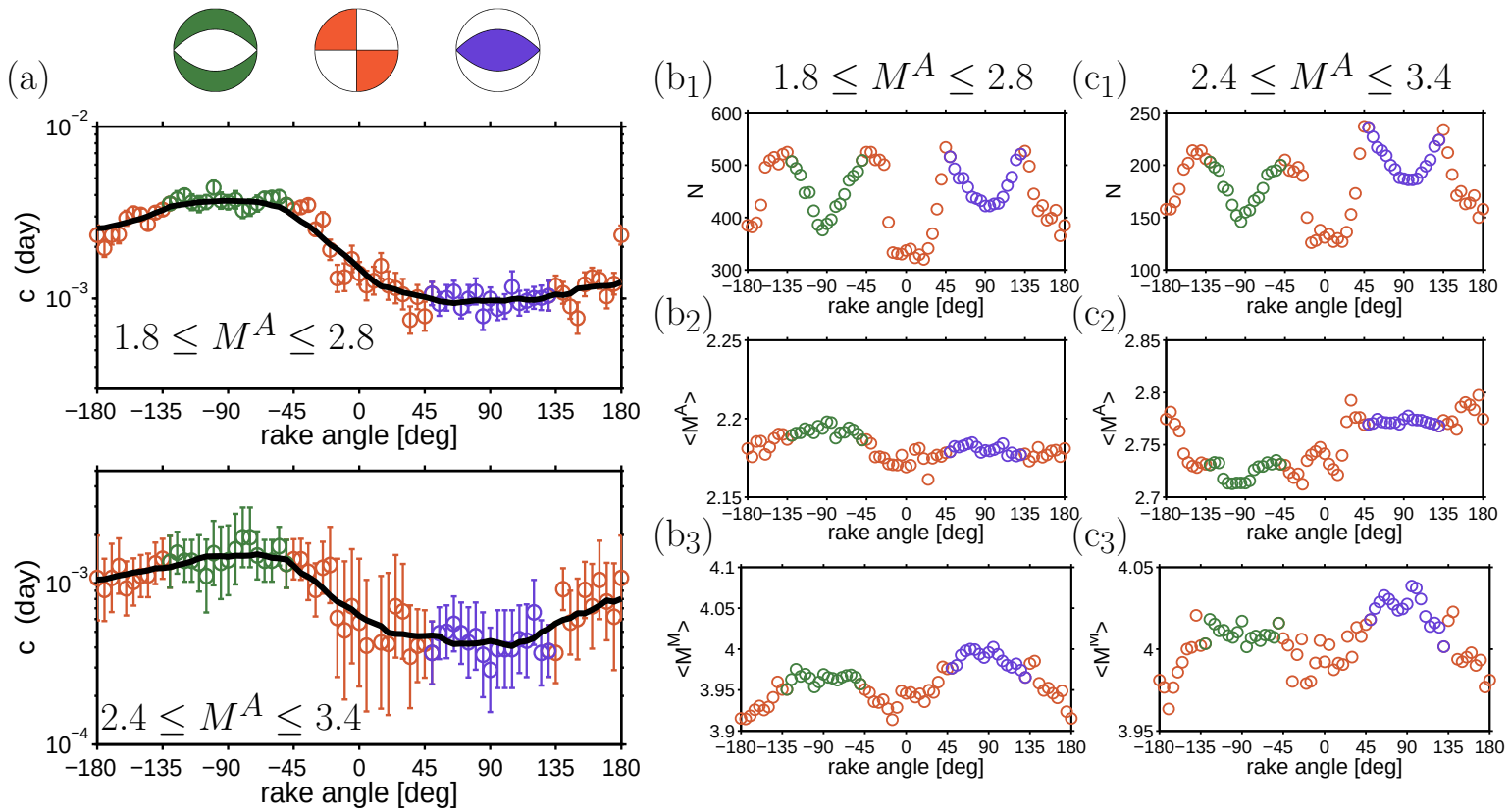

Figure 15: **(a)** the logarithm of the c-value with respect to both rake angles for aftershock-magnitude ranges of $[1.8; 2.8]$ (top) and $[2.4; 3.4]$ (bottom) in Japan. Red, green and blue distinguish rake intervals of mainly strike-slip, normal, and thrust events, respectively. Error bars are estimated by a Monte Carlo method and correspond to 16% and 84% quantiles of the maximum-likelihood estimates of c for 500 synthetic aftershock sequences at each point. **(b)** and **(c)** show the number of selected aftershocks (b_1 and c_1), the average magnitude of selected aftershocks (b_2 and c_2), and selected main shocks (b_3 and c_3).

5 Statistical stability of the c-values

The selection of aftershocks require four parameters: two for the aftershock magnitude range $[M^{\mathrm{A}}_{\mathrm{min}}; M^{\mathrm{A}}_{\mathrm{max}}]$; one for the radius of influence, R; one for the maximum main shock magnitude, $M^{\mathrm{M}}_{\mathrm{max}}$. These 4 parameter values are determined from seismological and statistical constraints:

- The radius R has to be as small as possible in order to limit the perturbations due to seismic noise, but large enough to capture a significant number of aftershocks within the first day. Practically, we take $R = 0.02$ km according to the relationship between the magnitude and the rupture length [*Wells and Coppersmith*, 1994].
- The lower aftershock magnitude threshold $M^{\mathrm{A}}_{\mathrm{min}}$ is given by an absolute catalogue completeness [*Schorlemmer and Woessner*, 2008].
- The higher magnitude threshold $M^{\mathrm{A}}_{\mathrm{max}}$ is given from the $M^{\mathrm{A}}_{\mathrm{min}}$-value using a constant magnitude interval, Δ, determined according to the number of aftershocks in our catalogue ($\Delta = 1$ in the manuscript). Because the results depend on the aftershock magnitude range, it is always better to take the Δ-value as small as possible.
- The $M^{\mathrm{M}}_{\mathrm{max}}$-value is the magnitude for which the average magnitude of aftershocks ranging from 1.8 to 2.5 starts to increase due to an increase in catalogue incompleteness (see Fig. 1).

Here, we use some descriptive statistics to demonstrate that these parameters are not key for the dependency of the c-value on the rake angle. As in the previous section, we divide our aftershock catalogue into three subcatalogues according to λ, the rake angles of the main shocks: normal, strike-slip, and thrust earthquakes. Normal events have $-135° \leq \lambda \leq -45°$; strike-slip have $-45° \leq \lambda \leq 45°$, $-180° \leq \lambda \leq -135°$, and $135° \leq \lambda \leq 180°$; thrust have $45° \leq \lambda \leq 135°$. Then, we linearly explore the parameter space for the 4 parameters listed above:

- We vary $M^{\mathrm{A}}_{\mathrm{min}}$ from 1.4 to 3.0 in steps of 0.2.
- We vary $M^{\mathrm{A}}_{\mathrm{max}}$ from 2.5 to 4.0 in steps of 0.3.
- The radius of influence R expressed in kilometre is taken from the set $[0.005, 0.01, 0.02, 0.04, 0.08, 0.16, 0.32]$.
- We vary $M^{\mathrm{M}}_{\mathrm{max}}$ from 3.9 to 5.1 in steps of 0.2.

At 2576 locations within this parameter space, we estimate c-values for normal, strike-slip, and thrust events. Fig. 16 shows the cumulative distribution functions of these c-values. They can be clearly distinguished from one another, and the distributions for normal, strike-slip, and thrust events

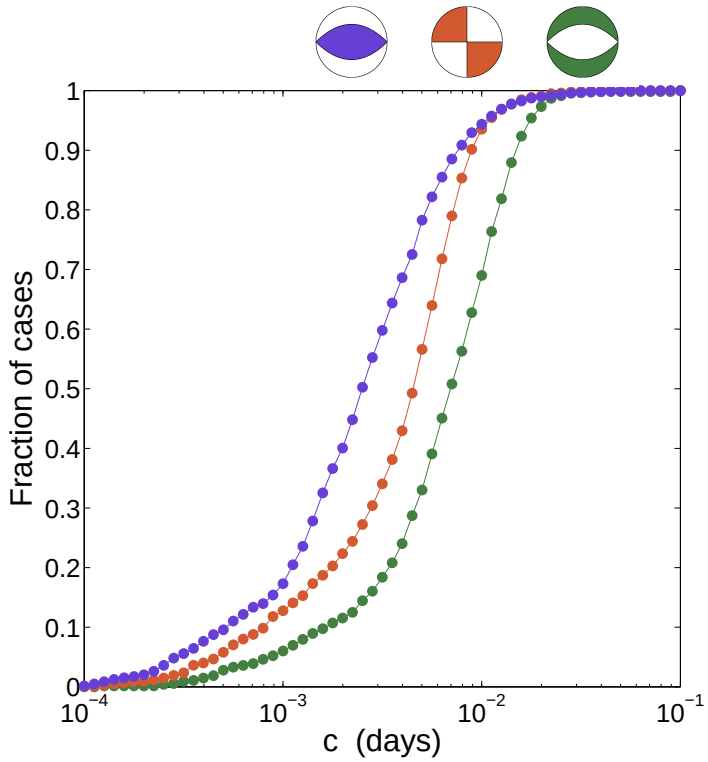

Figure 16: Cumulative distribution function of c-values calculated for normal (green), strike-slip (red), and thrust (blue) events at 2576 locations within the $\{R; M^{\rm A}_{\rm min}; M^{\rm A}_{\rm max}; M^{\rm M}_{\rm max}\}$ parameter space of the aftershock selection procedure (see text for the different values of these parameters).

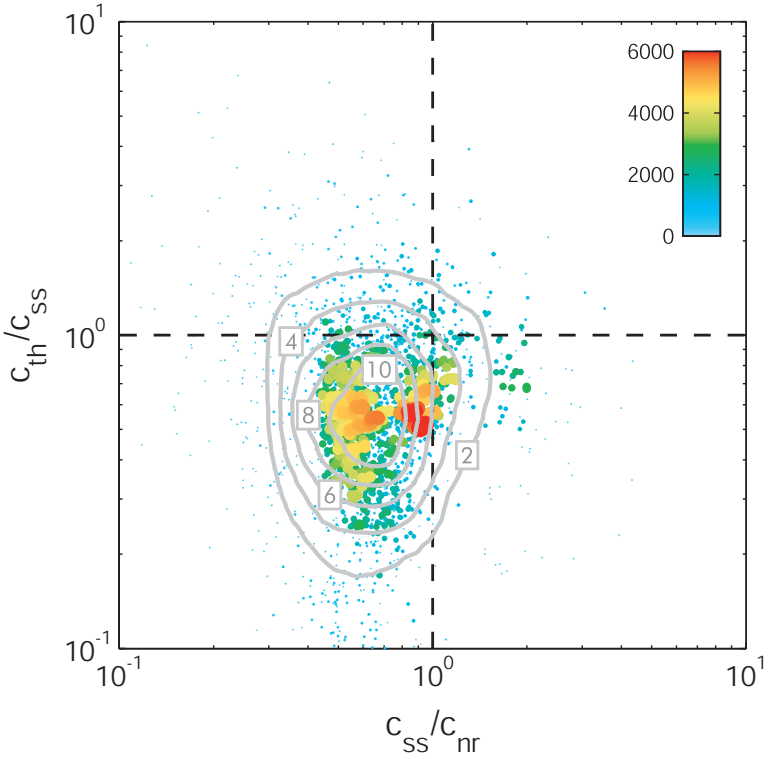

Figure 17: The ratio between the c-values for thrust ($c_{\rm th}$) and strike-slip events ($c_{\rm ss}$) with respect to the ratio between the c-values for strike-slip and normal events ($c_{\rm no}$). Each of the 2576 dots correspond to a particular set of parameter values within the parameter space of the aftershock selection procedure (see text). The color and size correspond to the cumulated number of events in the stacks. Contour lines limit areas of equal probability ($\times 10^4$) in the normalized density plot. This distribution shows that $c_{\rm no} > c_{\rm ss} > c_{\rm th}$ across the entire space of the parameters involved in the stacking procedure.

show significantly different c-values; large for normal events, intermediate for strike-slip, and small for thrust. The Kolmogorov-Smirnov test shows that these three distributions are different with errors smaller than 10^{-4}.

At each individual location in the parameter space of the model, we also compare c-values between different faulting styles. Fig. 17 shows that in a vast majority of cases the c-value is decreasing going from normal to strike-slip ($c_{\rm no}/c_{\rm ss} < 1$) and from strike-slip to thrusts events ($c_{\rm th}/c_{\rm ss} < 1$). Therefore, we conclude that the results obtained in the manuscript do not show significant variations due to the choice of parameters for aftershock selection.

References

Gardner, J., and L. Knopoff, Is the sequence of earthquakes in southern California with aftershocks removed Poissonian?, *Bull. Seismol. Soc. Am.*, *5*, 1363–1367, 1974.

Hauksson, E., Crustal structure and seismicity distribution adjacent to the Pacific and North America plate boundary in southern California, *J. Geophys. Res.*, *105*, 13,875–13,903, 2000.

Kilb, D., V. Martynov, and F. Vernon, Aftershock detection as a function of time: results from the ANZA seimic network following the 31 October 2001 M_{L} 5.1 Anza, California, earthquake, *Bull. Seism. Soc. Am.*, *97*, 780–792, 2007.

Nanjo, K. Z., B. Enescu, R. Shcherbakov, D. L. Turcotte, T. Iwata, and Y. Ogata, Decay of aftershock activity for Japanese earthquakes, *J. Geophys. Res.*, *112*, B08,309, 2007.

Narteau, C., P. Shebalin, and M. Holschneider, Temporal limits of the power law aftershock decay rate, *J. Geophys. Res.*, *107*, 2002.

Peng, Z. G., J. E. Vidale, M. Ishii, and A. Helmstetter, Seismicity rate immediatly before and after main shock rupture from high frequency waveforms in Japan, *J. Geophys. Res.*, *112*, 2007.

Reasenberg, P., Second-order moment of central California seismicity, 1969-1982, *J. Geophys. Res.*, *90*, 5479–5495, 1985.

Scholz, C., Microfractures, aftershocks, and seismicity, *Bull. Seismol. Soc. Am.*, *58*, 1117–1130, 1968.

Schorlemmer, D., and J. Woessner, Probability of detecting an earthquake, *Bull. Seismol. Soc. Am.*, *98*, 2103–2117, 2008.

Schorlemmer, D., S. Wiemer, and M. Wyss, Variations in earthquake-size distribution across different stress regimes, *Nature*, *437*, 539–542, 2005.

Shcherbakov, R., D. L. Turcotte, and J. B. Rundle, A generalized Omori's law for earthquake aftershock decay, *Geophys. Res. Lett.*, *31*, 2004.

Wells, D. L., and K. J. Coppersmith, New empirical relationships among magnitude, rupture length, rupture width, rupture area and surface displacement, *Bull. Seismol. Soc. Am.*, *84*, 974–1002, 1994.